Research Article

METTL14 Regulates Intestine Cellular Senescence through m⁶A Modification of Lamin B Receptor

Zizhen Zhang [1,2,3] **Meng Xue,** [1,2,3] **Jingyu Chen,** [1,2] **Zhuo Wang,** [1,2,3] **Fangyu Ju,** [1,2] **Jiaojiao Ni,** [1,2] **Jiawei Sun,** [1,2] **Haoyue Wu,** [4] **Huimei Zheng,** [4] **Ziwei Lou,** [4] **Yawen Zhang,** [3,5] **Xiaohang Yang,** [4] **Shujie Chen** [3,5] **Yongmei Xi** [4] **and Liangjing Wang** [1,2,3]

[1]*Department of Gastroenterology, The Second Affiliated Hospital of Zhejiang University School of Medicine, Zhejiang, China*
[2]*Institute of Gastroenterology, Zhejiang University, Zhejiang, China*
[3]*Research Center of Prevention and Treatment of Senescent Disease, Zhejiang University School of Medicine, Hangzhou, China*
[4]*The Woman's Hospital and the Institute of Genetics, Zhejiang University School of Medicine, Zhejiang, China*
[5]*Department of Gastroenterology, Sir Run Run Shaw Hospital, Zhejiang University School of Medicine, Zhejiang, China*

Correspondence should be addressed to Yongmei Xi; xyyongm@zju.edu.cn and Liangjing Wang; wangljzju@zju.edu.cn

N-6-Methyladenosine (m⁶A) modification is involved in multiple biological processes including aging. However, the regulation of m⁶A methyltransferase-like 14 (METTL14) in aging remains unclear. Here, we revealed that the level of m⁶A modification and the expression of METTL14 were particularly decreased in the intestine of aged mice as compared to young mice. Similar results were confirmed in *Drosophila melanogaster*. Knockdown of Mettl14 in *Drosophila* resulted in a short lifespan, associated disrupted intestinal integrity, and reduced climbing ability. In human CCD-18Co cells, knockdown of METTL14 accelerated cellular senescence, and the overexpression of METTL14 rescued senescent phenotypes. We also identified the lamin B receptor (LBR) as a target gene for METTL14-mediated m⁶A modification. Knockdown of METTL14 decreased m⁶A level of LBR, resulted in LBR mRNA instability, and thus induced cellular senescence. Our findings suggest that METTL14 plays an essential role in the m⁶A modification-dependent aging process via the regulation of LBR and provides a potential target for cellular senescence.

1. Introduction

Aging is a systematic biological process which causes physiological deficits leading to many age-associated disorders including neurodegenerative diseases, cancer, and cardiovascular disease [1–4]. Recent studies have implicated a variety of epigenetic changes that occurs during the aging process [5], including histone methylation, histone acetylation [6], DNA methylation [7], and RNA modification [8]. N-6-Methyladenosine (m6A) is the most prominent epigenetic modification in messenger RNAs (mRNAs) and noncoding RNA (ncRNA) [9]. It plays pivotal roles in biological processes such as stemness maintenance, differentiation, and cell senescence [10, 11].

The m⁶A modification in RNA is a reversible chemical modification. It is regulated by the methyltransferase complex consisting of m⁶A "writers" (including METTL3, METTL14, and WTAP), m⁶A "erasers" (including FTO and ALKBH5), and m⁶A "readers" (including YTHDC1, YTHDC2, YTHDF1, YTHDF2, and HNRNPC) [12–14]. The downstream functions of m6A are mediated by reader proteins that regulate mRNA processing [15]. IGF2BP2, IGF2BP3, and YTHDF1 are a class of m6A readers which promote the stability of mRNAs [16–18]. Besides, there are various other regulations including mRNA stability, translational regulations, pre-mRNA splicing, and RNA nuclear export [12].

Previous studies have shown that METTL3/14 is progressively declined in cells that have undergone replicative senescence [19]. Global m6A modification level is also notably reduced in prematurely senescent human mesenchymal stem cells (hMSCs) [20]. Further studies found that depletion of METTL3 led to m⁶A modified *MIS12*

mRNA downregulation, thus accelerating hMSC senescence [20]. Global m[6]A modification mainly occurs in mRNAs, and a subset of methylated mRNAs are subsequently decreased in old cohorts compared to young cohorts [21].

Lamin B receptor (LBR) is an evolutionary conserved, multifunctional protein [22]. Previous studies have shown that knockdown of LBR facilitates cellular senescence in HeLa cells and induces cellular senescence in normal human diploid fibroblasts [23]. Lack of LBR caused chromatin structure changes and altered metabolic and inflammatory processes, resulting in physiological aging [24]. Knockdown of LBR could upregulate the expression of the senescence-associated secretory phenotype (SASP) factors such as IL-6 and IL-8 in HeLa cells [25]. Recent study indicated the reduction of LBR by miR-340-5p as a mechanism whereby WI-38 human diploid fibroblasts promote senescence by reducing chromatin stability [26]. Studies also demonstrated that cytoplasmic chromatin foments (CCF), a senescence-associated proinflammatory program, underscore the important and novel role for LBR in maintaining heterochromatin homeostasis and avoiding senescence [27].

The intestine is an organ which undergoes considerable degeneration corresponding to the aging process [28, 29], whilst remaining indispensable for food digestion, nutrient absorption, and waste removal [30]. Upon aging, the intestinal barrier function becomes weakened, and the ability of digestion and absorption undergoes a corresponding decline. *Drosophila* is a useful model organism for studies on human aging [31]. For example, both *Drosophila* models and human studies have shown similarly increased intestinal permeability with aging [32, 33]. However, whether m[6]A RNA modification plays a role in gut senescence has not yet been well elucidated.

In this study, using mice, *Drosophila*, and a colon fibroblast-CCD18-Co cell line as models, we explored the effects of m[6]A modification on the gut function and cellular senescence. The m[6]A modification level showed considerable decreased in 18-month mice gut tissues comparing with those of 3-month mice. Knockdown of METTL14 in CCD18-Co cells also showed characteristics of accelerated senescence. Correspondingly, flies with Mettl14 depletion had a shorter lifespan and disrupted intestinal integrity. We concluded that METTL14 exerts a regulatory function via m[6]A modification in LBR RNA during aging that is highly correlated to cellular senescence.

2. Materials and Methods

2.1. Cell Culture and DOX-Induced Senescent Cells. The colon fibroblast cell line CCD-18Co was purchased from American Type Culture Collection (ATCC, Manassas, VA, USA). The cell line was cultured in Eagle's Minimum Essential Medium (EMEM; Genom, Hangzhou, China) supplemented with 10% fetal bovine serum (FBS; Sijiqing, Hangzhou, China) and 1% penicillin and streptomycin. The cell line was cultured in a monolayer culture in a humidified atmosphere containing 5% CO_2 at 37°C. For senescence induction, cells were plated at a density of 200,000 per well of a six-well plate. For induction of

senescence by doxorubicin (DOX; Sigma-Aldrich, St. Louis, MO, USA), CCD-18Co cells were cultured in the presence of 300 nM doxorubicin in complete culture media for 72 h. CCD18-Co cells were cultured to a confluent state and counted. Population doubling level (PDL) during each passage was calculated by the equation $A = 3.32 (\log N2 - \log N1) + X$ (A, added population doubling level; N2, collected cell number at the end of each passage; and N1, cell number at the beginning of each passage). Cells were passaged until they did not show obvious proliferation (usually passage 18–20), which could be considered as high passage. Cells at higher passages and DOX-induced senescent cells were used for analysis.

2.2. Plasmid Construction and Lentivirus Preparation. For the METTL14 overexpression, the METTL14 coding region was inserted into a pLV-puro plasmid (GeneChem, Shanghai, China). For METTL14 or LBR knockdown, lentiviral vector (GV248) containing METTL14 or LBR was obtained from GeneChem (Shanghai, China). The shRNA sequences were listed in Table 1. HEK 293 T cells were transfected with abovementioned plasmids and the virus packing plasmids using PolyJet transfection reagent (SignaGen, Rockville, MD, USA). The virus-containing medium was harvested and filtered to remove cell debris after 48 h. CCD-18Co cell line was plated in six-well plates. 24 hours later, the cell lines were transduced with virus-containing medium to establish stably infected cell lines.

2.3. Reverse Transcription-Quantitative PCR (RT-qPCR). For RT-qPCR assays, total RNA was extracted using the TRIzol® Reagent (Invitrogen, Camarillo, CA, USA) following the manufacturer's protocols, and then, a total of $1 \mu g$ RNA was converted into cDNA using PrimeScript™ RT Reagent Kit (Takara, Japan) according to the manufacturer's instructions. RT-qPCR was carried out using SYBR Premix Ex Taq (Takara, Japan) in a Light Cycler®480 Real-Time PCR System (Roche) using cDNA. The cDNA was then quantified using real-time PCR under the following conditions: denaturation at 95°C for 2 min, 40 cycles of 95°C for 15 s, and 60°C for 30 s. The primer sequence of related genes involved in the article is listed in Table 2. The $2^{-\Delta\Delta Ct}$ method was applied to calculate the relative mRNA expression. β-Actin served as internal normalized reference.

2.4. Western Blotting. Total proteins were extracted from CCD-18Co cells using a RIPA lysis buffer. The concentration of extracted proteins was measured using the BCA standard method (Beyotime Institute of Biotechnology Corp., Shanghai, China). Samples containing equal amounts of proteins were electrophoresed using sodium dodecyl sulphate polyacrylamide gel electrophoresis (SDS-PAGE) on 10% gels and transferred to a polyvinylidene fluoride (PVDF) membranes. After blocking with 5% BSA solutions for 2 h at room temperature, membranes were incubated using the following antibodies: LBR (diluted 1 : 500, ab32535; Abcam, Cambridge, UK), p53 (diluted 1 : 1000, ab26; Abcam), p21 (diluted 1 : 1000, ab109199; Abcam), p16 (diluted 1 : 1000, ET1602-9; HUABIO, Hangzhou, China), METTL14 (diluted 1 : 1000, 26158-1-AP; Proteintech, Wuhan, China), WTAP (diluted 1 : 1000,

TABLE 1: Sequences of shRNAs (5′-3′).

sh-NC	GGTTCTCCGAACGTGTCACGT
sh-METTL14#1	CCATGTACTTACAAGCCGATA
sh-METTL14#2	GCCGTGTTAAATAGCAAAGAT
sh-LBR#1	TGATTGGATGGGTGGTTATTA
sh-LBR#2	TTCCCACCAGGCCGACATTAA

60188-1-Ig; Proteintech), ALKBH5 (diluted 1 : 1000, 16837-1-AP; Proteintech), YTHDC1 (diluted 1 : 1000, A7318; ABclonal, Wuhan, China), YTHDC2 (diluted 1 : 1000, A15004; ABclonal), METTL3 (diluted 1 : 1000, db318; Diagbio, Hangzhou, China), and β-actin (as the loading control) (diluted 1 : 1000, 3700; CST, Danvers, USA) at 4°C overnight. They were then washed three times with TBST and then incubated with secondary antibody conjugated to horse radish peroxide (HRP) (diluted 1 : 5000, A0208; Beyotime, Shanghai, China). Specific immune complexes were exposed with ECL Western Blotting Substrate (NCM Biotech, Suzhou, China) and detected using the Syngene GeneGenius gel imaging system (Syngene, Cambridge, UK).

2.5. *m^6A Dot Blot Assay.* Total RNA isolated from tissues or cells, as described above, was dissolved in 3 times volume of RNA incubation buffer and denatured at 65°C for 5 min. Then, the samples were divided into subgroups of 200 ng, 100 ng, or 50 ng. These were dissolved in SSC buffer (Sangon Biotech, Shanghai, China), loaded to an Amersham Hybond-N+ membrane (GE, Healthcare, USA) which was settled on the Bio-Dot Apparatus (Bio-Rad, USA). The membrane was then crosslinked by UV light for 5 min, followed by staining with 0.02% methylene blue (Sangon Biotech, China). The membranes were scanned to indicate the total content of input RNA. After blocking with 5% skimmed milk, membranes were incubated with specific m^6A antibody (diluted 1 : 1000, #202003; Synaptic System, Germany) overnight at 4°C. Following washing, the membranes were incubated with HRP-conjugated anti-rabbit immunoglobulin G (IgG) for 2 h before being visualized using the imaging system. The results of dot blotting were obtained using Syngene GeneGenius gel imaging system (Syngene, Cambridge, UK) and quantified by ImageJ. Methylene blue (MB) staining was used as loading control.

2.6. *RNA Decay Assay.* To measure RNA stability, an RNA decay assay was performed. CCD-18Co cell line was cultured in three 6-well plates followed by the treatment of METTL14 knockdown. Actinomycin D (Selleck, S8964) was added into each well at a final concentration of 5 μg/ml. Cells were collected at 0, 2, or 4 h. Total RNA was extracted, and qPCR was performed to quantify the relative abundance of *LBR* mRNA (relative to 0 h).

2.7. *Methylated RNA Immunoprecipitation (MeRIP).* m^6A antibody (Synaptic System; #202003) and normal rabbit IgG (Beyotime Biotechnology, #A7028) were conjugated to protein A/G mixed magnetic beads, respectively (Beyotime Biotechnology, #A7016), overnight at 4°C. Total RNA was

TABLE 2: Information of the RT-qPCR primers.

Primers	Sequencing (5′-3′)
Mouse β-actin-F	TGGCTCCTAGCACCATGAAG
Mouse β-actin-R	CGCAGCTCAGTAACAGTCCG
Mouse Mettl14-F	CTTCGACCGAAGTCACCTCC
Mouse Mettl14-R	CTACCGAGGAGTAAAGCCGC
Mouse Mettl3-F	GATAGTCCCGTGCCTACTGC
Mouse Mettl3-R	TGGCGTAGAGATGGCAAGAC
Mouse Wtap-F	CATTTTGTGGCTGCGAGACC
Mouse Wtap-R	TCTGTTTCACTCAGTCGGACC
Mouse Alkbh5-F	CTTTGCTTCGGCTGCAAGTT
Mouse Alkbh5-R	AATGTCCTGAGGCCGTATGC
Mouse Ythdc1-F	CGTAGGAAGCTGAGTGGAGC
Mouse Ythdc1-R	TCCCCATCTTTCTCCTCCCG
Mouse Ythdc2-F	GCTCATGCAATGATGACCTGT
Mouse Ythdc2-R	AATGCCATTGTTGAGTCGCC
Drosophila RP49-F	TGGTTTCCGGCAAGCTTCAA
Drosophila RP49-R	TGTTGTCGATACCCTTGGGC
Drosophila Mettl14-F	AGGAAGAGGAGTTTGGCAGC
Drosophila Mettl14-R	GCTGGAGCCTCAGCAAAGTA
Drosophila Mettl4-F	TACTGCACCAACTTCTGCCC
Drosophila Mettl4-R	AGCTTCGAGAGCGGTATGTG
Drosophila Mettl3-F	GCACAAAAGTCGAGTGCCTG
Drosophila Mettl3-R	CTGCCGATTCTGTCTTGGGT
Drosophila fl(2)d-F	GTGGTATTGGAGGAGTGTATGC
Drosophila fl(2)d-R	CGATTGCTTCGTTATCTCTGGC
Drosophila Ythdc1-F	GCGAAAAGTAGCGAGAGAAAGC
Drosophila Ythdc1-R	GGTTTGGCACACACGATACA
Human β-actin-F	AGAGCTACGAGCTGCCTGAC
Human β-actin-R	AGCACTGTGTTGGCGTACAG
Human FBL-F	GCCCACACCTTCCTGCGTAATG
Human FBL-R	TGCGGCTTCATGTTCTCCTGTTG
Human ITPRIPL1-F	TGAGCAGAGGCAGAAGGCAGAG
Human ITPRIPL1-R	GTTCCACAGGTTTCCCAGCATCC
Human LBR-F	GGAAGTTAAATTGACTCCGCTG
Human LBR-R	AGGTGCGTCATTTCTCTCAATA
Human FAM129A-F	GCAACAGAGGACACAGCAGGAC
Human FAM129A-R	CAAAGAACCCGAGGCAGTGATGG
Human MCUB-F	GGATATCATGGAGCCAGTTACA
Human MCUB-R	TCAGGGATTCTTTAGCCTTAGC
Human SSRP1-F	GTCTGTTTTTGTTACCCCACAA
Human SSRP1-R	TTCTTCCTCGTTCATGTTCAGA
Human TMSB15A-F	GCCAGACTTGTCGGAAGTGG
Human TMSB15A-R	TGCTGGATAGTTTCCTTTGAGGGA
Human HIST1H1D-F	TGTGAAGAAAAAGGCGAAGAAG
Human HIST1H1D-R	GCCTTGGTGATAAGCTCAGATA
Human CDCA7L-F	GTCAGATTTGAGTGATGATGGC
Human CDCA7L-R	TTTTCTCATTCTGTAAGCGTGC
Human CBS-F	ACCATCGAGATCCTCCGGGA
Human CBS-R	GGGACGAGAGCATGTTCCCA

Table 2: Continued.

Primers	Sequencing (5′-3′)
Human *HIST1H1A*-F	GAAGGCAAAGAAACCTGCTAAG
Human *HIST1H1A*-R	CTCTTAATGCCCAGCTTAATGC
Human *HIST1H1E*-F	CTCATTACTAAAGCTGTTGCCG
Human *HIST1H1E*-R	TGTTGTTCTTCTCCACGTCATA
Human *PTMA*-F	AGGTGATGGTGAGGAAGAGGA TGG
Human *PTMA*-R	CTCGTCGGTCTTCTGCTTCTTGG
Human *ANP32B*-F	GGCTTAACAGCTGAATTTGTGA
Human *ANP32B*-R	TTGGGGAGATTTGAAACTGAGA
Human *CBX2*-F	GACTTAGATGCTAAGAGGGGTC
Human *CBX2*-R	CTTCTTCCGGATGGGATCCTTC
Human *HIST2H2AB*-F	GCCATCTGCAACTAGCCGTGAG
Human *HIST2H2AB*-R	TTGTTCTTGCCAGGCTTGTGACTC
Human *PARP1*-F	CGGAGTCTTCGGATAAGCTCT
Human *PARP1*-R	TTTCCATCAAACATGGGCGAC
Human *H3FF*-F	GGATACCAACCTGTGCGCCATT
Human *H3FF*-R	GGACAGACTTCTTGGGCTGATAG
Human *H2BH*-F	CAAGGTGCTGAAGCAAGTCCAC
Human *H2BH*-R	TGGAGGTGATGGTCGAACGCTT

incubated with the antibody in immunoprecipitation buffer supplemented with RNase inhibitor overnight at 4°C. RNA was then eluted from the beads and extracted, and the m6A-enriched RNA and the input reversely transcribed into cDNA. Enrichment was detected by qPCR. Relative enrichment of m6A was normalized to the input: %input = 1/$2^{Ct [IP]-Ct [Input]}$.

2.8. Cell Proliferation. To determine the clonal expansion efficiency of the cells from the different treatment groups, 2000 cells were seeded in 6-well plate. About 10-15 days later, the cells were fixed with 4% paraformaldehyde for 15 min and then stained with 0.2% crystal violet staining solution (Beyotime Institute of Biotechnology Corp., Shanghai, China) for 20 min at room temperature. Crystal violet was then eluted using 10% acetic acid, and the OD was examined at 595 nm using a spectrophotometer.

2.9. SA-β-Gal Staining. SA-β-Gal activity was measured using a SA-β-Gal staining kit (Beyotime Institute of Biotechnology Corp., Shanghai, China). Specifically, cells were washed three times with PBS and fixed for 15 min at room temperature for 15 min in the fixing solution of the SA-β-Gal kit. After washing in PBS three times, cells were incubated in senescence detection solution overnight at 37°C. The cells were then observed under a light microscope. SA-β-Gal activity was expressed as the percentage of SA-β-Gal staining-positive cells to total cells.

2.10. Immunofluorescence Staining. Immunofluorescence experiments were performed as follows. CCD-18Co cells were grown on coverslips. Cells were fixed for 15 min at room temperature (RT) in a 4% paraformaldehyde solution

before being permeablized by PBS with 0.1% Triton-X-100 for 10 min at RT. Coverslips were then washed with PBS and blocked with 5% BSA in PBS. Primary antibody was incubated for 2 h and secondary antibody for 1 h at room temperature. An anti-m6A antibody (#202003) was used at 1 μg/ml for immunofluorescence. Alexa 568-conjugated anti-rabbit (diluted 1:200, Invitrogen, USA) was used as the secondary antibodies for immunofluorescence analysis.

2.11. Animals. The C57BL/6 mice used in this experiment were obtained from SLAC Laboratory Animal Co. Ltd. (Shanghai, China) and housed in a specific pathogen-free (SPF) level room. The room temperature was maintained at 22°C with 12 h light/dark cycle. Mice were provided with ad libitum water and food. All animal studies were performed in accordance with the guidelines of the Institutional Animal Use and the Animal Experimentation Ethics Committee of Zhejiang University School of Medicine (20161206-21). The following fly strains were used: w[1118], tubulin-Gal4, and UAS-Mettl14-RNAi.

2.12. Fly Lifespan Assay. Flies were reared on standard cornmeal medium at 25°C. Progeny was reared at standard density under 12L:12D at 25°C and 70% humidity. Adult flies were collected in standard culture vials with a maximum of 10 flies per vial. Flies were counted daily and transferred to fresh vials every other day. The lifespan of the fly was calculated as the number of days it survived postemergence.

2.13. Climbing Assay. In brief, cohorts of 20 flies of the indicated age and genotype were transferred into two empty vials which were connected at their opening with adhesive tape, creating an enclosed transparent tube, approximately 15 cm tall. After the transfer, flies were allowed to rest for 30 minutes at room temperature. The tubes were then tapped to bring all the flies to the bottom. The movement of the flies during the experiments was recorded using a digital camera. The number of flies passing the 8 cm mark on the vial over 20 seconds was counted. For each cohort of 30 flies, the experiment was repeated 3 times. A total of two cohorts from separate crosses were analyzed and scored for each group.

2.14. Smurf Assay. Gut barrier function was analyzed by placing flies on blue food (FD&C blue dye#1, E8500 blue dye, Solarbio, Beijing, China) postfeeding [34]. Briefly, each group was transferred onto fresh medium containing blue dye (2.5% w/v) at 8 a.m. for 12 h. "Smurf" flies were defined by visible blue food dye seen throughout the body (not limited to the proboscis and crop), which suggests disruption of gut integrity. A fly was counted as "Smurf positive" when blue dye could be observed outside of the digestive tract [35].

2.15. Statistical Analysis. Data was expressed as mean ± standard deviation. Student's test was used to analyze the differences between two groups. A one-way ANOVA or two-way ANOVA analysis was used to compare the differences among more than two groups. A p value <0.05 was regarded statistically significant. Statistical analyses were performed using the GraphPad Prism 8.0 Software (GraphPad, Inc., San Diego, USA).
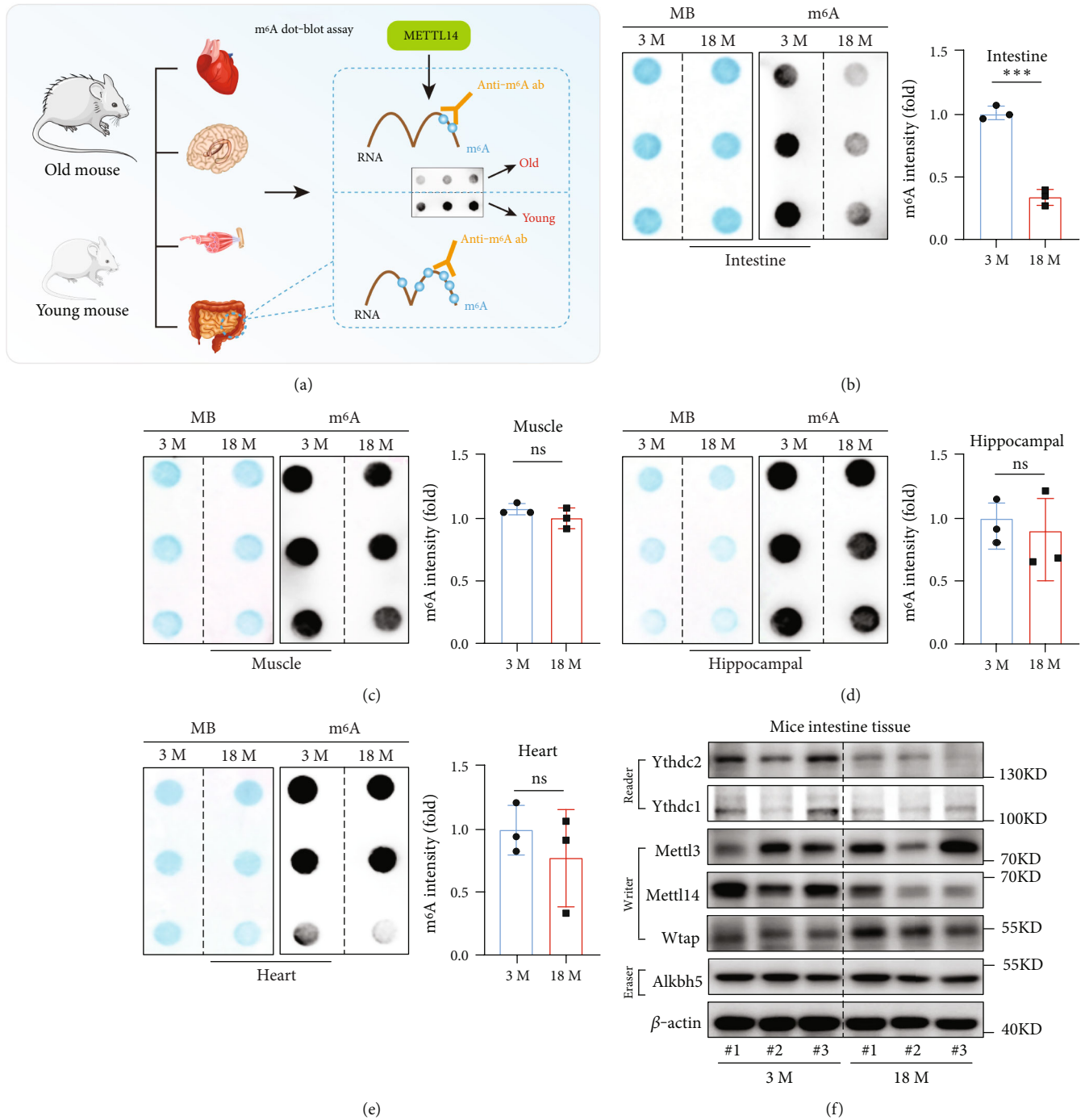
(a)

(b)

(c)

(d)

(e)

(f)

FIGURE 1: m⁶A modification and the expression of Mettl14 were downregulated in the colon along with the aging process. (a) Flow diagram of the study design. (b–e) The m⁶A modification levels in the intestine, muscle, hippocampus, and heart collected from 3-month and 18-month old mice were tested by m⁶A dot blot assays. Methylene blue staining (left) was used to detected input RNA, while the intensity of dot immunoblotting (right) represents the level of m⁶A modification. Data are expressed as mean ± SD of three independent biological experiments. Student t-test. ns: not significant; ***$p < 0.001$. (f) The protein expression level of the key enzyme of m⁶A modification in intestines from old (18 month) or young (3 month) mice.

3. Results

3.1. The m⁶A Modification and the Expression Level of Mettl14 Were Decreased in Aged Mice and Drosophila.
To investigate whether m⁶A modification level changes with aging, we firstly performed m⁶A dot blot assay to detect m⁶A level in various tissues of 18-month or 3-month old mice (Figure 1(a)). Results showed that m⁶A level was decreased in colon tissues of 18-month-old mice as compared to that of 3-month-old mice but not in other tissues from the muscle, hippocampus, or heart (Figures 1(b)–1(e)). The decreased m⁶A level could be related to the
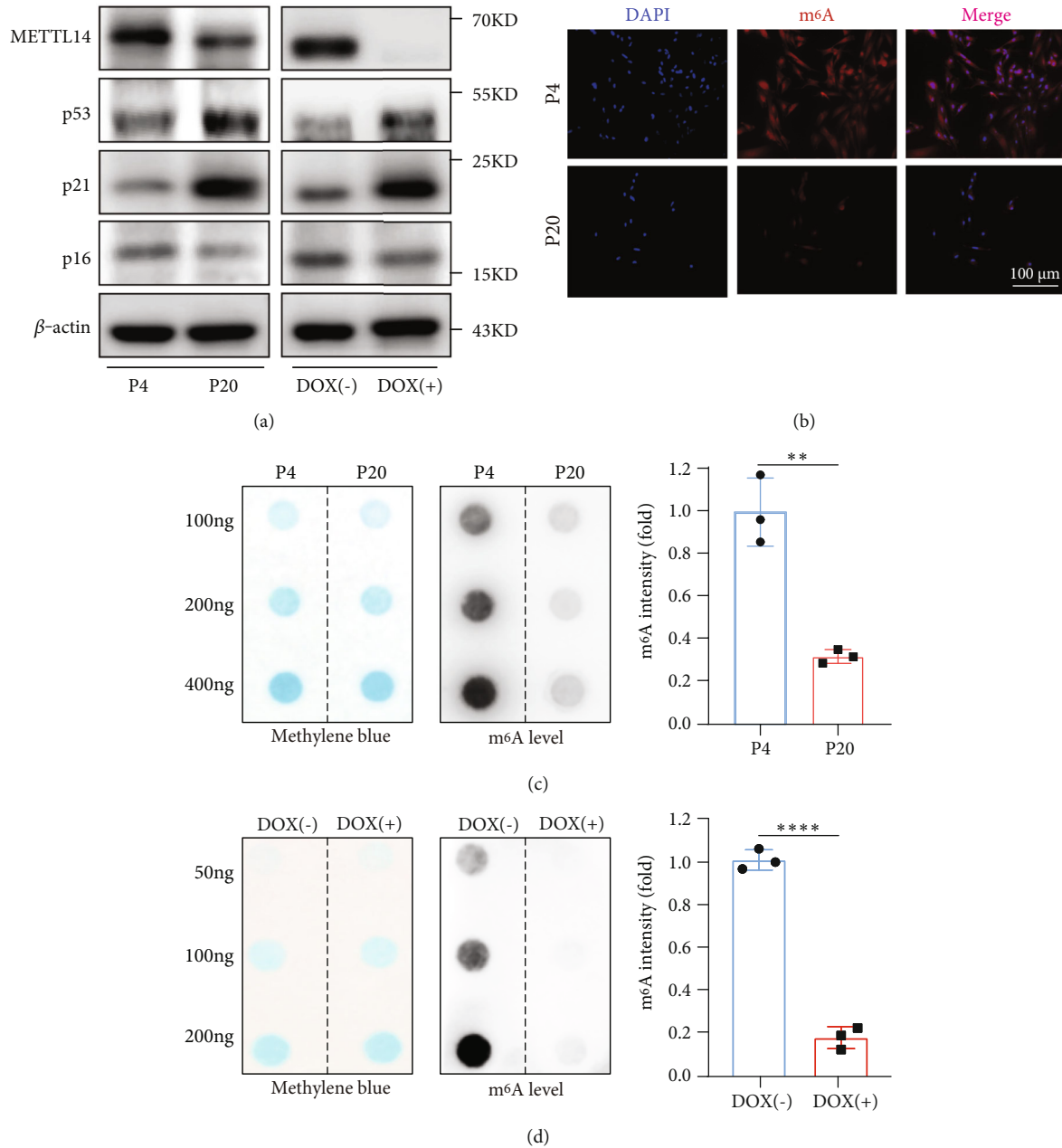
(a)

(b)

(c)

(d)

FIGURE 2: Alteration of m^{6}A modification level and METTL14 expression with aging. (a) Western blot analysis of METTL14 protein levels in two cellular models. (b) Immunofluorescence analyses were conducted to evaluate the m^{6}A modification levels at different passages. Scale bar, 100 μm. (c) Global m^{6}A level of RNA extracted from different passages cells was measured via m^{6}A dot blot assays. RNAs were serially diluted and loaded equally with 100 ng, 200 ng, or 400 ng. Data are expressed as mean ± SD of three independent biological experiments. Student t-test. $^{**}p < 0.01$. (d) Global m^{6}A level of RNA extracted from DOX-induced senescent CCD18-Co cells was measured via m^{6}A dot blot assays. RNAs were serially diluted and loaded equally with 50 ng, 100 ng, or 200 ng. Methylene blue staining (left) was used to detected input RNA, while the intensity of dot immunoblotting (right) represented the level of m^{6}A modification. Data are expressed as mean ± SD of three independent biological experiments. Student t-test. $^{****}p < 0.0001$; P4: passage 4; P20: passage 20; DOX: doxorubicin.

dysregulation of the m^{6}A methylase complex or demethylases [36]. Western blot analysis of key enzymes showed that the expression of Mettl14 was significantly downregulated in intestine tissues of 18-month mice, compared to that in the 3-month group (Figure 1(f)), which were consistent with the qPCR data (Figure S1A). To examine whether Mettl14 was downregulated during aging in other organisms, we analyzed the m^{6}A modification levels in flies and found

that the mRNA expression of *Mettl14* was significantly decreased in 40-day old flies as compared to that in 5-day old flies (Figure S1B). These observations suggest that decreased Mettl14 expression levels are associated with the aging process.

3.2. The Modification of m^{6}A Was Downregulated in Senescent Cells. CCD-18Co, a colon fibroblast cell line [37],
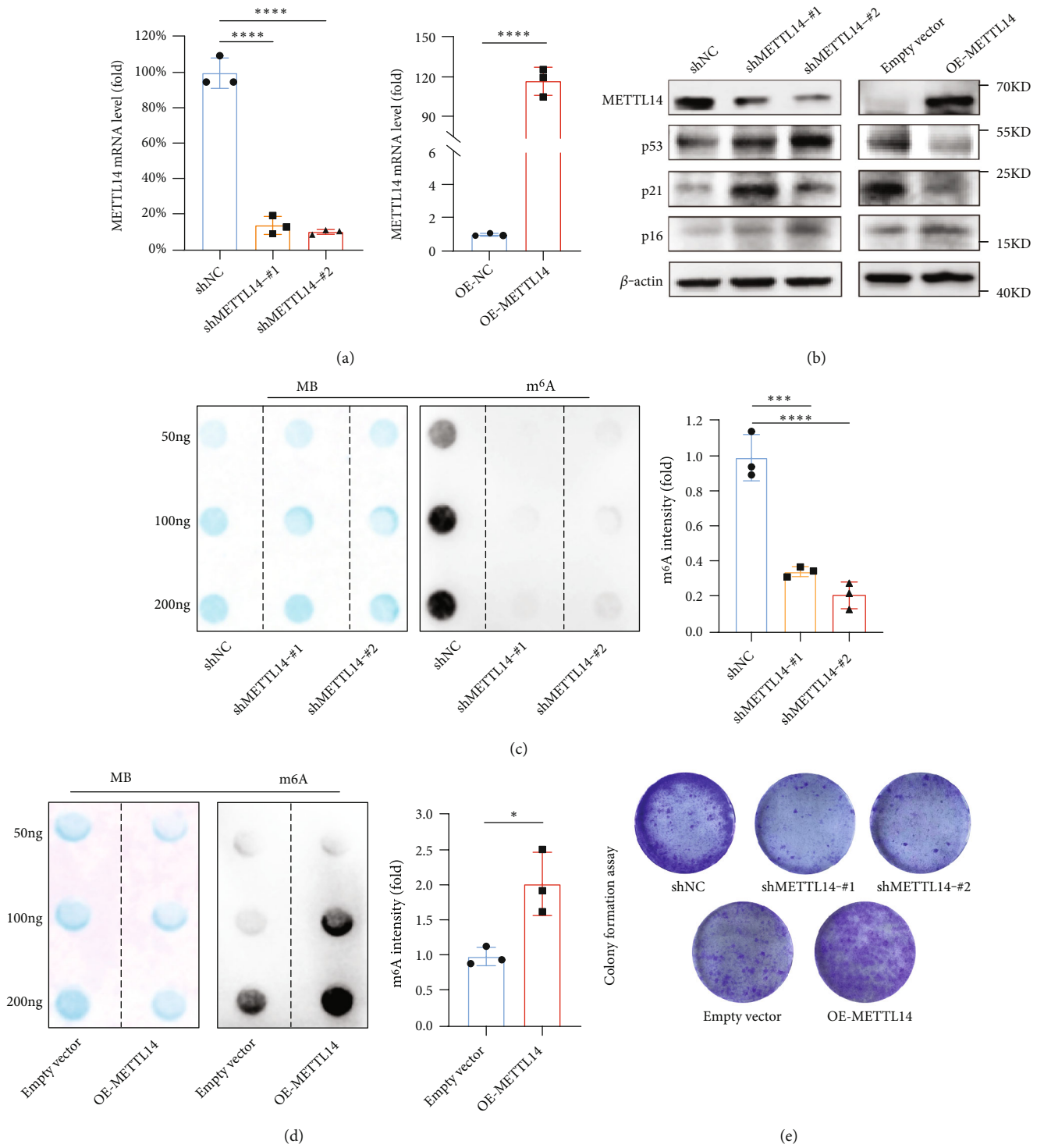
(a)

(b)
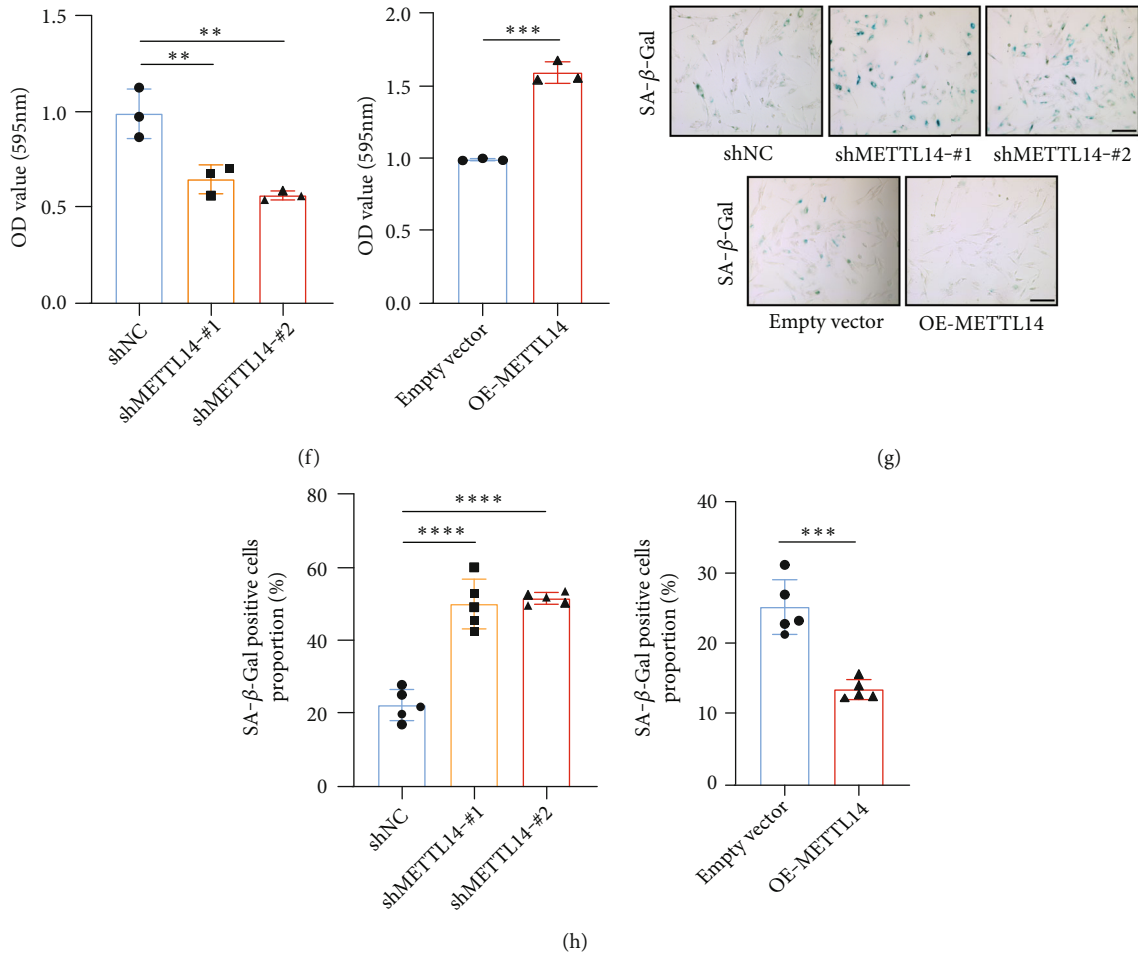
(c)

(d)

(e)

Figure 3: Continued.

(f)

(g)

(h)

FIGURE 3: Functional analysis of the METTL14 role in cellular senescence. (a, b) The mRNA and protein expression levels of METTL14 were measured by RT-qPCR and western blotting, respectively, after transfection with the shRNA targeting METTL14 plasmid and pLV-METTL14 plasmid. β-Actin was used as the internal control. Data are expressed as mean ± SD of three independent biological experiments. Student t-test. $^{****}p < 0.0001$. (c, d) Global m^6A level of RNA extracted from METTL14-silenced or METTL14-overexpressed CCD18-Co cells was measured using dot blot assays. RNAs were loaded equally to 50 ng, 100 ng, or 200 ng. Data are expressed as mean ± SD of three independent biological experiments. One-way ANOVA followed by Tukey's test (c). Student t-test (d). $^{***}p < 0.001$; $^{*}p < 0.05$. (e, f) Colony formation assay in METTL14-silenced or METTL14-overexpressed CCD18-Co cells. The stained cells were eluted using 10% acetic acid, and the absorbance of extracted strain was measured at 595 nm to quantify. Data were presented as mean ± SD, $n = 6$. One-way ANOVA followed by Tukey's test (e). Student t-test (f). $^{**}p < 0.01$; $^{***}p < 0.001$. (g, h) Analysis of SA-β-Gal activity in METTL14-silenced or METTL14-overexpressed CCD18-Co cells. Scale bar, 200 μm. Data were presented as mean ± SD, $n = 5$. One-way ANOVA followed by Tukey's test (g). Student t-test (h). $^{***}p < 0.001$; $^{****}p < 0.0001$.

was used to evaluate the effect of m^6A modification on cellular senescence. As shown in Figure S2A, the proliferation of CCD-18Co had slowed down along with the passage number, suggesting that passage 4 (P4) cells were in a relatively juvenile status, while passage 20 (P20) cells were senescent. CCD-18Co cells were treated with doxorubicin to generate drug-inducible senescence. An inhibited clone formation ability indicated the successful establishment of senescent cell model (Figure S2A). We also performed SA-β-Gal staining, one of the primary criteria for identifying senescent cells. A higher proportion of senescent cells were observed than that in control cells (Figure S2B).

We then examined the expression of METTL14 in the cells, showing downregulated METTL14 protein levels in both the replicative and inducible senescence cell models. The expression level of p53 and p21, which were markers

of senescence, was negatively correlated with that of METTL14 (Figure 2(a)). An m^6A modification level was also analyzed using immunofluorescence. As expected, the m^6A level was reduced in cells of a higher passage number (Figure 2(b)). We further detected m^6A methylation by m^6A mRNA dot blot and found that the overall m^6A level declined both with increasing passages and upon DOX-induced cellular senescence (Figures 2(c) and 2(d)).

3.3. METTL14 Regulates m^6A Modification-Dependent Colon Fibroblast Senescence. We generated METTL14-silenced or METTL14-overexpressed cell lines using short hairpin RNA (shRNA) or overexpression plasmids (Figures 3(a) and 3(b)), respectively. shRNA-mediated METTL14 knockdown led to a significant upregulation of p53 and p21 in CCD18-Co cells, while the METTL14 overexpression
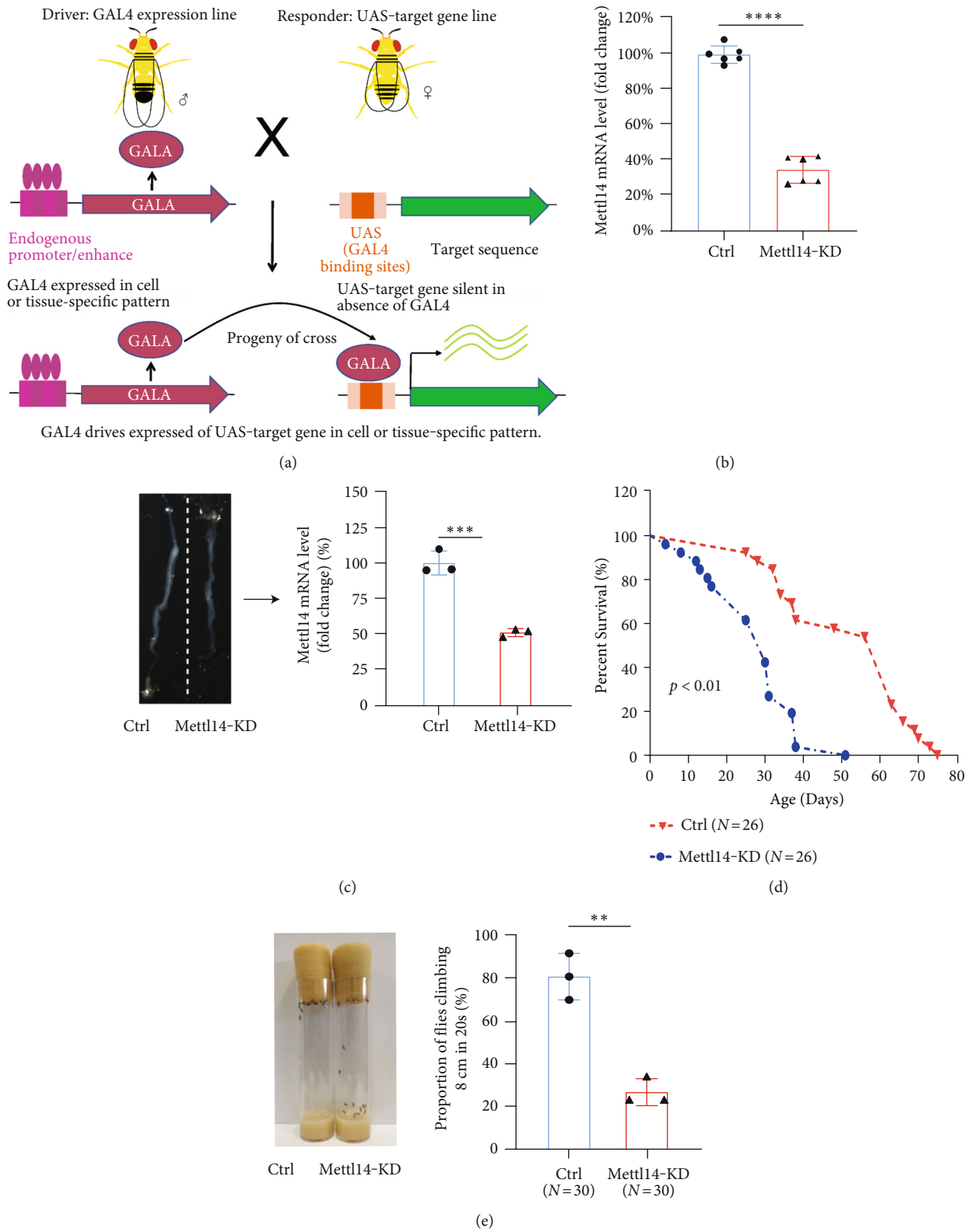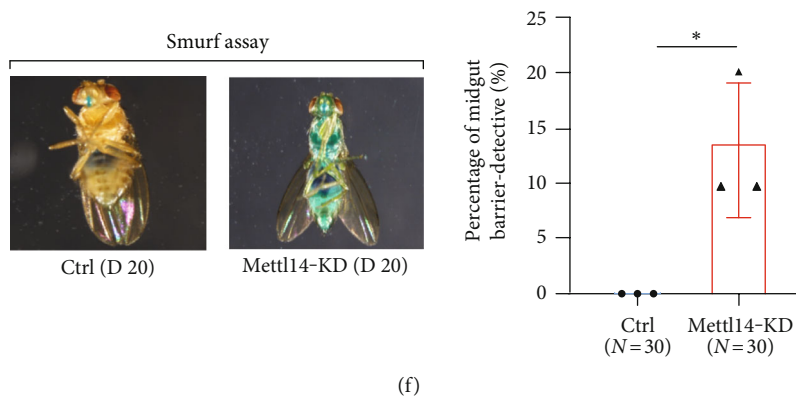
(a)

(b)

(c)

(d)

(e)

Figure 4: Continued.

(f)

FIGURE 4: Knocking down Mettl14 shortens lifespan and increases intestinal permeability. (a) *UAS-Mettl14 RNAi* and *tubulin-GAL4* flies were intercrossed to generate *UAS-Mettl14 RNAi* and *tubulin-GAL4* flies. In the *GAL4-UAS* system, the transcription activator protein GAL4 binds to the upstream activation sequence (*UAS*) and activates *Mettl14 RNAi* transcription to knock down Mettl14 in *Drosophila melanogaster*. (b) The knockdown efficiency of *Mettl14* in transgenic flies was tested by RT-qPCR. Data are expressed as mean ± SD of three independent biological experiments. Student *t*-test. ****$p < 0.0001$. (c) Verification of intestine dissected from transgenic flies *Mettl14* knockdown by RT-qPCR. left is a dissection showing the *Drosophila* intestinal tract. Data are expressed as mean ± SD of three independent biological experiments. Student *t*-test. ***$p < 0.001$. (d) Survival curves of control and transgenic flies. The log-rank (Kaplan-Meier) test was performed. (e) Comparison of climbing ability of control and transgenic flies at day 20. Data are expressed as mean ± SD of three independent biological experiments. Student *t*-test. **$p < 0.01$. (f) Smurf gut permeability assay in 20-day old control and *Mettl14 RNAi* flies. Data are expressed as mean ± SD of three independent biological experiments. Student *t*-test. *$p < 0.05$.

considerably reduced the expressions of p53 and p21 (Figures 3(a) and 3(b)). We then applied dot blot assays to determine the effects of METTL14 on m⁶A methylation level. Results showed that both METTL14 knockdown and overexpression significantly affected the m⁶A methylation level (Figures 3(c) and 3(d)), implying that METTL14 was critical for m⁶A modification. In addition, METTL14-silenced CCD-18Co cells acquired characteristics of premature ageing, as shown by decreased proliferative capacity and increased percentage of SA-β-Gal-positive cells. These results indicated that whilst METTL14 knockdown accelerated CCD-18Co senescence, its overexpression enhanced cell proliferation capacity and reduced the numbers of SA-β-Gal-positive cells (Figures 3(e)–3(h)). Collectively, METTL14 was confirmed to play a vital role in the m⁶A modification-dependent colon fibroblast senescence.

3.4. Knockdown of Mettl14 Led to Shorter Lifespan and Disrupted Intestinal Barrier in Drosophila. To investigate the role of METTL14-mediated m⁶A modification in aging, we performed Mettl14 knockdown experiments in *Drosophila* (Figure 4(a)). The silencing efficiency of *Mettl14* was validated by RT-qPCR using the whole fly sample (Figure 4(b)). We dissected gastrointestinal tracts of the flies and examined *Mettl14* expression levels. A significantly downregulated level was noted in the intestine tissues of *Mettl14* knockdown flies, as compared with that in controls (Figure 4(c)).

In *Drosophila*, climbing ability was measured to evaluate locomotor behavior, so we evaluated the lifespan together with climbing ability of the flies (Figure S3). Results showed that Mettl14 knockdown flies had a short lifespan (Figure 4(d)) and exhibited a weaker creep ability than control flies (Figure 4(e)). This correlated with the suggestion that the loss of intestinal integrity could be used as an organismal aging marker for flies [38]. We performed Smurf assay in

Mettl14 knockdown flies and observed that knockdown of Mettl14 disrupted intestinal integrity, with significantly increased Smurf-positive flies, compared to the controls (Figure 4(f)). These results suggested that Mettl14 played an essential role in regulating locomotor behavior, intestinal integrity, and aging in *Drosophila*.

3.5. LBR Was Identified as an m⁶A-Targeted Gene. The Myriam Gorospe group, aimed to identify robust shared markers of senescence, performed RNA-sequencing analysis across 8 diverse models of senescence triggered in human diploid fibroblasts (WI-38, IMR-90) and endothelial cells (HUVEC, HAEC) by replicative exhaustion, exposure to ionizing radiation or doxorubicin, and expression of the oncogene HRAS-G12V [39]. On the basis of the data (GSE130727) presented above, the same data was reanalyzed. Considering that there was a positive correlation between m⁶A modification levels and mRNA expression levels [20], we focused on protein-coding genes that were downregulated in nine comparison groups. Using a Venn diagram, a total of 19 common candidate key genes were unveiled. We then conducted RT-qPCR to evaluate the impact of METTL14 on each candidate gene. Among these, LBR was significantly downregulated following METTL14 silencing (Figure 5(a)). We further confirmed that METTL14 knockdown resulted in decreasing LBR protein level in CCD18-Co cells and the overexpression of the METTL14 enhanced LBR expression (Figure 5(b)). These data indicated that *LBR* could be a target gene of METTL14.

To identify the specific m⁶A methylation loci of *LBR*, we interrogated the *LBR* sequence using the SRAMP website (http://www.cuilab.cn/sramp/) [40] and screened out 2 positions with a likely abundance of m⁶A methylation loci (Figure 5(c)). We also found that METTL14 knockdown induced a quicker degradation rate of *LBR* mRNA

List 1: WI38 Doxorubicin-induced senescence-1
List 2: WI38 IR-induced senescence
List 3: WI38 replicative senescence
List 4: HAEC IR-induced senescence
List 5: HUVEC IR-induced senescence
List 6: IMR90 IR-induced senescence
List 7: IMR90 replicative senescence
List 8: WI38 Doxorubicin-induced senescence-2
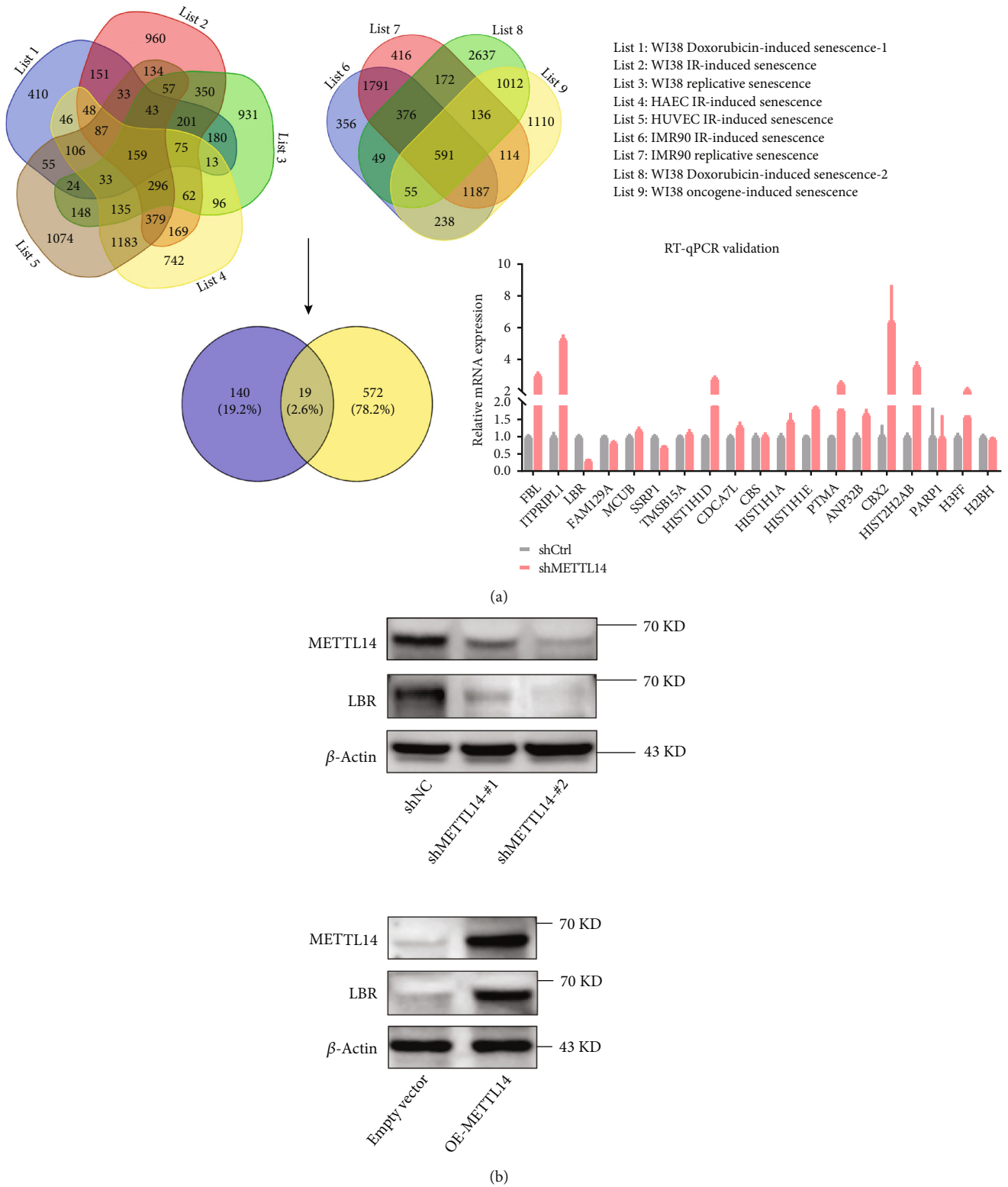List 9: WI38 oncogene-induced senescence

(a)

(b)

FIGURE 5: Continued.

(c)

(d)

(e)
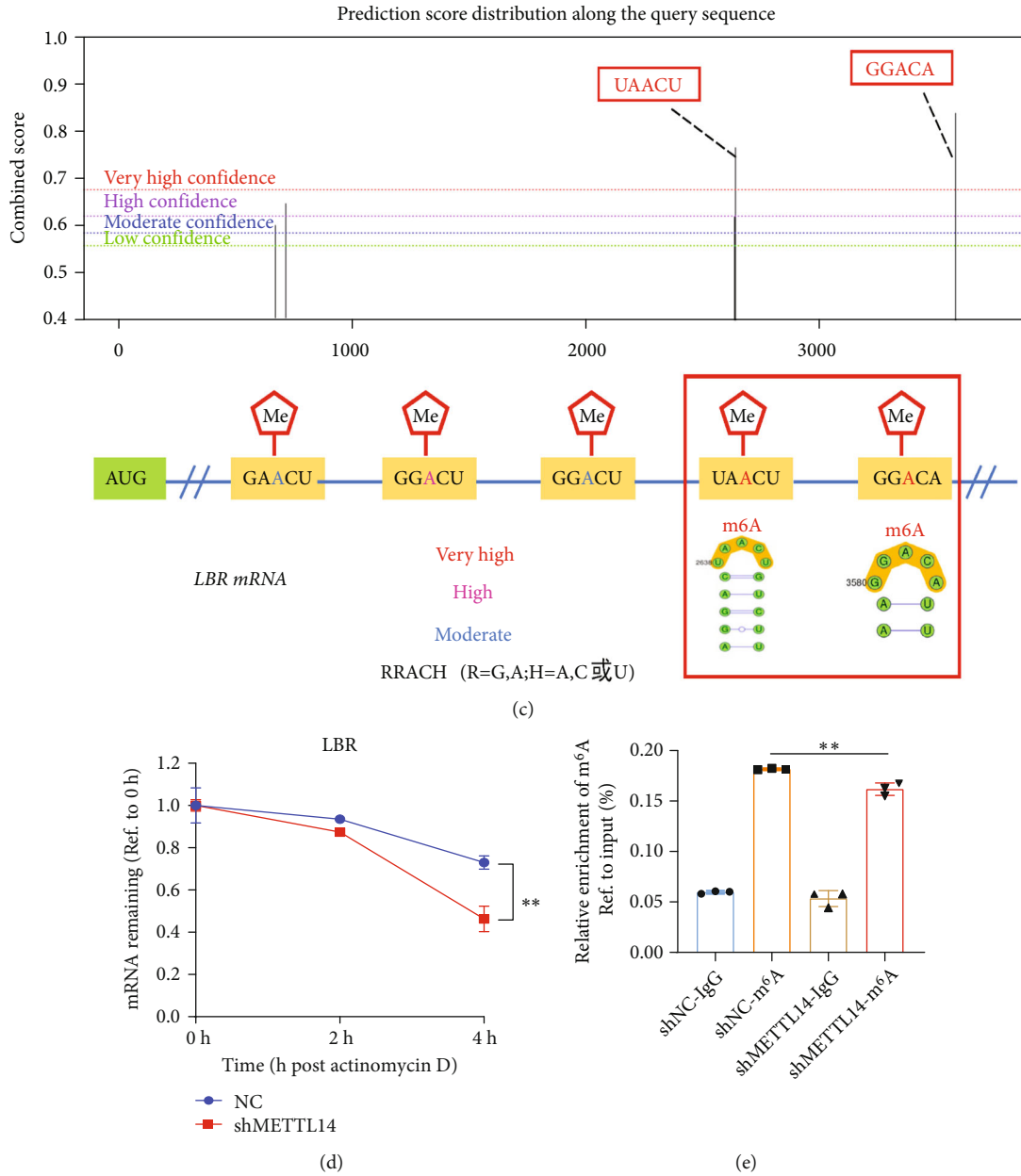
FIGURE 5: *LBR* is a key downstream gene of METTL14. (a) Schematic diagram showing the screening criterion for METTL14 targets. Venn diagram of all the possible overlapping transcripts in nine comparison groups sequenced together, showing reduced abundance with senescence and filtering for a significant FDR < 0.15. RNA-seq data was acquired from GEO datasets (GSE130727). RT-qPCR was performed in CCD18-Co with METTL14 knockdown to validate the overlapped genes. The *LBR* was consistent among 19 genes. *FBL*: fibrillarin; *ITPRIP*: inositol 1,4,5-trisphosphate receptor interacting protein; *LBR*: lamin B receptor; *FAM129A*: family with sequence similarity 129 member A; *MCUB*: mitochondrial calcium uniporter dominant negative subunit beta; *SSRP1*: structure specific recognition protein 1; *TMSB15A*: thymosin beta 15A; *HIST1H1D*: H1.3 linker histone, cluster member; *CDCA7L*: cell division cycle associated 7 like; *CBS*: cystathionine beta-synthase; *HIST1H1A*: H1.1 linker histone, cluster member; *HIST1H1E*: H1.4 linker histone, cluster member; *PTMA*: prothymosin alpha; *ANP32B*: acidic nuclear phosphoprotein 32 family member B; *CBX2*: chromobox 2; *HIST2H2AB*: histone cluster 2 H2A family member B; *PARP1*: poly(ADP-ribose) polymerase 1; *H3FF*: H3 clustered histone 11; *H2BH*: H2B clustered histone 9. (b) The expression of LBR following METTL14 knockdown or overexpression was evaluated by western blotting. (c) Prediction of the specific m⁶A methylation loci of *LBR* using the SRAMP website. (d) METTL14-silenced cells were treated with actinomycin D and harvested at 0, 2, or 4 h. RNA decay rates were determined to estimate the stability of *LBR* mRNA (normalized to the expression at 0 h). Data are expressed as mean ± SD of three independent biological experiments. Two-way ANOVA analysis. $^{**}p < 0.01$. (e) m⁶A modification of *LBR* was detected by MeRIP-qPCR analysis using anti-IgG and anti-m⁶A antibodies. Relative m⁶A enrichment of *LBR* mRNA for each IP group was normalized to input. Data are expressed as mean ± SD of three independent biological experiments. One-way ANOVA followed by Tukey's test. $^{**}p < 0.01$.
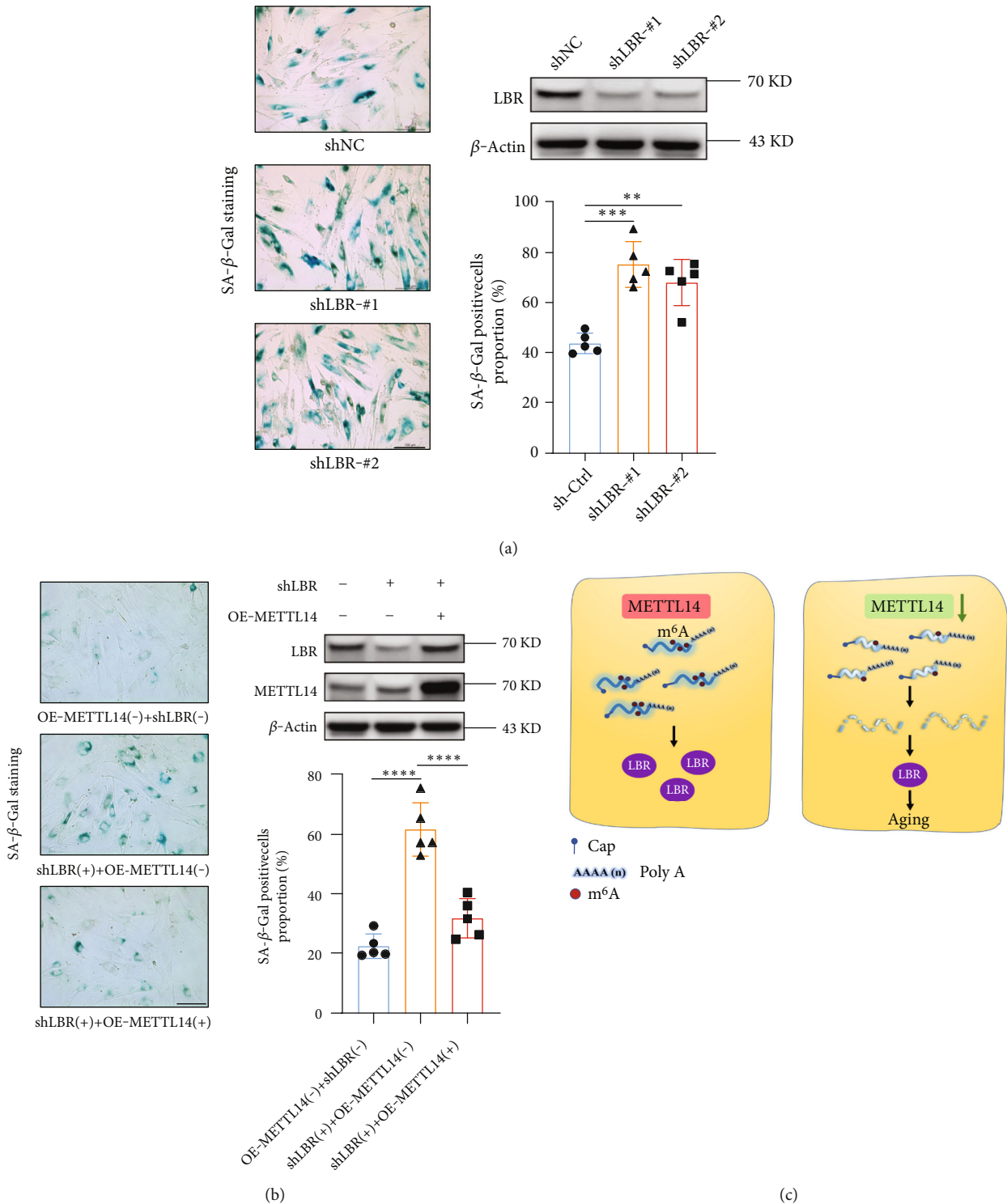
(a)

(b)

(c)

FIGURE 6: METTL14 delayed aging via stabilizing *LBR* mRNA. (a) Induction of cellular senescence in CCD18-Co cells by knocking down LBR. Western blotting was applied to detect the transfection efficiency of METTL14 shRNA. β-Actin was used as the internal control. The percentage of SA-β-Gal-positive cells was manually counted. Scale bar, 200 μm. Data were presented as mean $\pm$ SD, $n = 5$, biologically independent experiments. One-way ANOVA followed by Tukey's test. $^{**}p < 0.01$; $^{***}p < 0.001$. (b) The efficiency of the cotransfection of METTL14 overexpression plasmid and *LBR* shRNA into CCD18-Co cells was verified by western blotting. Rescue experiments were conducted to determine the influence of LBR knockdown on METTL14 overexpression cells, with bar charts showing the percentage of SA-β-Gal-positive cells. Data were presented as mean $\pm$ SD, $n = 5$, biologically independent experiments. One-way ANOVA followed by Tukey's test. $^{****}p < 0.0001$. (c) A schematic illustration to summarize our findings relating to METTL14-guided m6A modulation on LBR. METTL14 could maintain m6A levels to stabilize *LBR* mRNA. Contrastingly, METTL14 downregulation resulted in reduced *LBR* m6A levels, together with cellular senescence.

(Figure 5(d)). Therefore, we conducted a MeRIP-qPCR assay to determine the enrichment of m[6]A in *LBR*. Compared with IgG control, the m[6]A-specific antibody had robustly enriched *LBR* transcripts. There was a decreased amount of *LBR* modified by m[6]A following METTL14 knockdown (Figure 5(e)). Collectively, these results indicate that *LBR* could be a potential target gene of METTL14 in the m[6]A modification-dependent way.

3.6. METTL14 Delayed the Cellular Senescence through the Regulation of LBR. To uncover the role of LBR in regulating cell senescence, we performed LBR-specific shRNA knockdown in CCD-18Co cells. The SA-*β-Gal* staining showed that LBR knockdown clearly increased the ratios of blue-stained cells compared with those of the controls (Figure 6(a)). To investigate whether this phenotype was mediated by a dysregulation of the METTL14-LBR, CCD-18Co cells were cotransfected with an METTL14 overexpression plasmid and a shRNA plasmid targeting LBR. Western blotting analysis consistently verified the transfection efficiency. The SA-*β-Gal* staining assays showed that the ratios of blue-stained cells increased by LBR knocking down was reversed by transfection with METTL14 plasmid (Figure 6(b)).

4. Discussion

Over recent years, most developed countries have become increasingly prone to an aging population [41]. This may have paved the way for an increasing proportion of research focusing on molecular mechanisms associated with aging. An increase in intestinal permeability would allow bacterial components (e.g., LPS) to enter the bloodstream [42]. Growing evidence indicated that chronic inflammation accelerates senescence, while inflammation deletion delays senescence [43]. To our knowledge, disruption of the epithelial integrity allowed for enhanced permeability, bacterial translocation, and inflammation leading to inflammaging.

Growing evidence showed that m[6]A modification had an essential effect on some underlying diseases including cancers [42] and participated in multiple physiological and pathological processes by modulating different target pathways. m[6]A modification was essential for the maintenance of colonic epithelial homeostasis, and mice with colon-specific KO of Mettl14 showed disturbed integrity of the colonic epithelial barrier [43]. Wang et al. recently uncovered a novel antiviral function of m[6]A modification during rotavirus (RV) infection in small bowel intestinal epithelial cells (IECs) [44]. Similar study supported a model in which m[6]A modifications in the *Traf6* transcript regulated the intestinal immune response to bacterial infection via a complex consisting of *YTHDF1*, *DDX60*, and the *Traf6* transcript [45].

Epigenetic modifications have been suggested to play central roles in cell differentiation and senescence [46]. Lence et al. demonstrated that m[6]A modulates neuronal functions and sex determination in *Drosophila*, revealing that loss of function of the methyltransferases produced severe behavioral defects [47]. METTL3, in particular, was seen to be reduced in prematurely senescent hMSC models. Conversely, METTL3 was recognized as active in the alleviation of hMSC senescence

through m[6]A modification-dependent stabilization of the *MIS12* transcript [20].

We examined the m[6]A modification levels in a variety of mouse organs associated with different age groups. We found that the m[6]A modification level exhibited a particular decline in colon tissues of old mice. Zhang et al. had previously uncovered a unique m[6]A-regulation-expression pattern in the human brain and intestine tissues and confirmed m[6]A modification and enrichment to be organ-specific processes [48]. Similarly, as m[6]A regulators, the altered expression of METTL3 and METTL14 has been observed in various diseases and age-related processes where METTL3/14 was observed as progressively and notably declined in human F2S fibroblasts undergoing replicative senescence [19]. METTL14 is also a noted participator in the regulation of T cell homeostasis [49], and its knockdown in embryonic mouse brains disturbed embryonic cortical neurogenesis [50].

In our study, METTL14 was identified to regulate m[6]A modification levels linked to senescence in animal models and in colon fibroblast cells. Our study confirmed *LBR* as a target gene of METTL14 and showed that the expression of LBR was altered via m[6]A modification in the process of cellular senescence. Specific RNA modification sites are essential for m[6]A modification [51]. m[6]A modification clearly exerts its biological function via interplay with binding proteins [52] to directly or indirectly affect RNA function [53]. We uncovered that the m[6]A modification might promote the mRNA stability of *LBR* via the regulation of METTL14. However, the specific modification sites in *LBR* and further validation was warranted. Interestingly, these reader proteins had very different dynamics among the different species. Ythdc1 genes showed different expression levels in different species. The gene expression of Ythdc1 was downregulated in *Drosophila* melanogaster while upregulated in mice intestine during aging process in RNA levels (Figure S1). Whether this process has any interplay with other m[6]A reader proteins such as IGF2BP1/2/3 [54–56] and YTHDF1 [18] requires further study.

In summary, our findings demonstrate that METTL14-mediated m[6]A modification can delay cellular senescence, potentially through enhancing the stability of *LBR* mRNA (Figure 6(c)). Our *Drosophila* model with Mettl14 depletion showed a shorter lifespan and disrupted intestinal integrity. Overall, our results might suggest a potential target for anti-aging therapies.

Data Availability

All data generated or analyzed during this study are available from the corresponding authors on reasonable request.

Conflicts of Interest

No potential conflicts of interest were disclosed.

Authors' Contributions

L.W., Y.M., and S.C. conceived the research idea and designed the study. Z. Z, M.X., Z.W., J.C., and F.J. carried out the experiments. J.N., J.S., H.W., H.Z., Z.L., Y.Z., and

X.Y. performed the data analysis. Z. Z and M.X. wrote the manuscript with input from coauthors. All authors critically revised and approved the final version of the manuscript. Zizhen Zhang, Meng Xue, Jingyu Chen, and Zhuo Wang contributed equally to this work and share first authorship.

Acknowledgments

Supplementary Materials

Figure S1: verification of Mettl14 alteration in the aging process. (A) The mRNA expression level of the key enzyme of m⁶A modification in mice intestines from different ages. Data are expressed as mean ± SD of three independent biological experiments. Student t-test. $^*p < 0.05$; $^{**}p < 0.01$. (B) The relative mRNA expression of m⁶A RNA modification regulators in *Drosophila* at day 5 and day 40. Data are expressed as mean ± SD of three independent biological experiments. Student t-test. $^{**}p < 0.01$; $^{****}p < 0.0001$. Figure S2: senescence-related phenotype. (A) Clonal formation assay of replicated and DOX-induced CCD18-Co. Data are expressed as mean ± SD of three independent biological experiments. Student t-test. $^{****}p < 0.0001$; P4: passage 4; P20: passage 20. (B) Representative images of SA-β-Gal staining of replicated and DOX-induced CCD18-Co. Scale bar, 200 μm. Data are presented as means ± SD, $n = 5$. Student t-test. $^{***}p < 0.001$; $^{****}p < 0.001$; P4: passage 4; P20: passage 20; DOX: doxorubicin. *(Supplementary Materials)*

References

[1] J. P. De Magalhães, "How ageing processes influence cancer," *Nature Reviews Cancer*, vol. 13, no. 5, pp. 357–365, 2013.

[2] M. T. Heemels, "Ageing," *Nature*, vol. 464, no. 7288, p. 503, 2010.

[3] F. Ping, N. Jiang, and Y. Li, "Association between metformin and neurodegenerative diseases of observational studies: systematic review and meta-analysis," *BMJ Open Diabetes Research & Care*, vol. 8, no. 1, article e001370, 2020.

[4] J. W. Shay and I. B. Roninson, "Hallmarks of senescence in carcinogenesis and cancer therapy," *Oncogene*, vol. 23, no. 16, pp. 2919–2933, 2004.

[5] H. A. Cruickshanks, T. McBryan, D. M. Nelson et al., "Senescent cells harbour features of the cancer epigenome," *Nature Cell Biology*, vol. 15, no. 12, pp. 1495–1506, 2013.

[6] P. Sen, P. P. Shah, R. Nativio, and S. L. Berger, "Epigenetic mechanisms of longevity and aging," *Cell*, vol. 166, no. 4, pp. 822–839, 2016.

[7] A. A. Johnson, K. Akman, S. R. Calimport, D. Wuttke, A. Stolzing, and J. P. De Magalhães, "The role of DNA methylation in aging, rejuvenation, and age-related disease," *Rejuvenation Research*, vol. 15, no. 5, pp. 483–494, 2012.

[8] A. M. Shafik, F. Zhang, Z. Guo et al., "N6-methyladenosine dynamics in neurodevelopment and aging, and its potential role in Alzheimer's disease," *Genome Biology*, vol. 22, no. 1, p. 17, 2021.

[9] D. Yang, J. Qiao, G. Wang et al., "N 6-Methyladenosine modification of lincRNA 1281 is critically required for mESC differentiation potential," *Nucleic Acids Research*, vol. 46, no. 8, pp. 3906–3920, 2018.

[10] S. Geula, S. Moshitch-Moshkovitz, D. Dominissini et al., "Stem cells. m6A mRNA methylation facilitates resolution of naïve pluripotency toward differentiation," *Science*, vol. 347, no. 6225, pp. 1002–1006, 2015.

[11] A. Maity and B. Das, "N6-methyladenosine modification in mRNA: machinery, function and implications for health and diseases," *The FEBS Journal*, vol. 283, no. 9, pp. 1607–1630, 2016.

[12] M. Frye, B. T. Harada, M. Behm, and C. He, "RNA modifications modulate gene expression during development," *Science*, vol. 361, no. 6409, pp. 1346–1349, 2018.

[13] Y. Yue, J. Liu, and C. He, "RNA N6-methyladenosine methylation in post-transcriptional gene expression regulation," *Genes & Development*, vol. 29, no. 13, pp. 1343–1355, 2015.

[14] Y. Yang, P. J. Hsu, Y. S. Chen, and Y. G. Yang, "Dynamic transcriptomic m⁶A decoration: writers, erasers, readers and functions in RNA metabolism," *Cell Research*, vol. 28, no. 6, pp. 616–624, 2018.

[15] I. A. Roundtree, M. E. Evans, T. Pan, and C. He, "Dynamic RNA modifications in gene expression regulation," *Cell*, vol. 169, no. 7, pp. 1187–1200, 2017.

[16] J. Z. Huang, M. Chen, D. Chen et al., "A peptide encoded by a putative lncRNA HOXB-AS3 suppresses colon cancer growth," *Molecular Cell*, vol. 68, no. 1, pp. 171–184.e6, 2017.

[17] Q. Wang, C. Chen, Q. Ding et al., "METTL3-mediated m6A modification of HDGF mRNA promotes gastric cancer progression and has prognostic significance," *Gut*, vol. 69, no. 7, pp. 1193–1205, 2020.

[18] Q. Wang, X. Guo, L. Li et al., "N⁶-methyladenosine METTL3 promotes cervical cancer tumorigenesis and Warburg effect through YTHDF1/HK2 modification," *Cell Death & Disease*, vol. 11, no. 10, p. 911, 2020.

[19] J. Zhang, Y. Ao, Z. Zhang et al., "Lamin A safeguards the m6A methylase METTL14 nuclear speckle reservoir to prevent cellular senescence," *Aging Cell*, vol. 19, no. 10, article e13215, 2020.

[20] Z. Wu, Y. Shi, M. Lu et al., "METTL3 counteracts premature aging via m6A-dependent stabilization of MIS12 mRNA," *Nucleic Acids Research*, vol. 48, no. 19, pp. 11083–11096, 2020.

[21] K. W. Min, R. W. Zealy, S. Davila et al., "Profiling of m6A RNA modifications identified an age-associated regulation of AGO2 mRNA stability," *Aging Cell*, vol. 17, no. 3, article e12753, 2018.

[22] A. L. Olins, G. Rhodes, D. B. Welch, M. Zwerger, and D. E. Olins, "Lamin B receptor: multi-tasking at the nuclear envelope," *Nucleus*, vol. 1, no. 1, pp. 53–70, 2010.

[23] R. Arai, A. En, Y. Takauji et al., "Lamin B receptor (LBR) is involved in the induction of cellular senescence in human cells," *Mechanisms of Ageing and Development*, vol. 178, pp. 25–32, 2019.

[24] S. Castro-Obregón, "Lamin B receptor: role on chromatin structure, cellular senescence and possibly aging," *The Biochemical Journal*, vol. 477, no. 14, pp. 2715–2720, 2020.

[25] A. En, Y. Takauji, D. Ayusawa, and M. Fujii, "The role of Lamin B receptor in the regulation of senescence-associated secretory phenotype (SASP)," *Experimental Cell Research*, vol. 390, no. 1, article 111927, 2020.

[26] A. B. Herman, C. Anerillas, S. C. Harris et al., "Reduction of lamin B receptor levels by miR-340-5p disrupts chromatin, promotes cell senescence and enhances senolysis," *Nucleic Acids Research*, vol. 49, no. 13, pp. 7389–7405, 2021.

[27] K. N. Miller, S. G. Victorelli, H. Salmonowicz et al., "Cytoplasmic DNA: sources, sensing, and role in aging and disease," *Cell*, vol. 184, no. 22, pp. 5506–5526, 2021.

[28] J. Song, S. E. Wolf, X. W. Wu et al., "Starvation-induced proximal gut mucosal atrophy diminished with aging," *JPEN Journal of Parenteral and Enteral Nutrition*, vol. 33, no. 4, pp. 411–416, 2009.

[29] P. L. Ogra, "Ageing and its possible impact on mucosal immune responses," *Ageing Research Reviews*, vol. 9, no. 2, pp. 101–106, 2010.

[30] A. M. Chin, D. R. Hill, M. Aurora, and J. R. Spence, "Morphogenesis and maturation of the embryonic and postnatal intestine," *Seminars in Cell & Developmental Biology*, vol. 66, pp. 81–93, 2017.

[31] J. E. Fleming, I. Reveillaud, and A. Niedzwiecki, "Role of oxidative stress in drosophila aging," *Mutation Research*, vol. 275, no. 3-6, pp. 267–279, 1992.

[32] T. Y. Ma, D. Hollander, V. Dadufalza, and P. Krugliak, "Effect of aging and caloric restriction on intestinal permeability," *Experimental Gerontology*, vol. 27, no. 3, pp. 321–333, 1992.

[33] W. M. Saweirs, D. J. Andrews, and T. S. Low-Beer, "The double sugar test of intestinal permeability in the elderly," *Age and Ageing*, vol. 14, no. 5, pp. 312–315, 1985.

[34] K. Kierdorf, F. Hersperger, J. Sharrock et al., "Muscle function and homeostasis require cytokine inhibition of AKT activity in drosophila," *Elife*, vol. 9, article e51595, 2020.

[35] C. Xu, H. W. Tang, R. J. Hung et al., "The septate junction protein Tsp2A restricts intestinal stem cell activity via endocytic regulation of aPKC and Hippo signaling," *Cell Reports*, vol. 26, no. 3, pp. 670–688.e6, 2019.

[36] H. Wang, X. Hu, M. Huang et al., "Mettl3-mediated mRNA m^{6}A methylation promotes dendritic cell activation," *Nature Communications*, vol. 10, no. 1, p. 1898, 2019.

[37] Y. Guo, J. L. Ayers, K. T. Carter et al., "Senescence-associated tissue microenvironment promotes colon cancer formation through the secretory factor GDF15," *Aging Cell*, vol. 18, no. 6, article e13013, 2019.

[38] M. Rera, R. I. Clark, and D. W. Walker, "Intestinal barrier dysfunction links metabolic and inflammatory markers of aging to death in drosophila," *Proceedings of the National Academy of Sciences of the United States of America*, vol. 109, no. 52, pp. 21528–21533, 2012.

[39] G. Casella, R. Munk, K. M. Kim et al., "Transcriptome signature of cellular senescence," *Nucleic Acids Research*, vol. 47, no. 21, p. 11476, 2019.

[40] Y. Zhou, P. Zeng, Y. H. Li, Z. Zhang, and Q. Cui, "SRAMP: prediction of mammalian N6-methyladenosine (m6A) sites based on sequence-derived features," *Nucleic Acids Research*, vol. 44, no. 10, article e91, 2016.

[41] M. G. Fehlings, L. Tetreault, A. Nater et al., "The aging of the global population: the changing epidemiology of disease and spinal disorders," *Neurosurgery*, vol. 77, Supplementary 1, pp. S1–S5, 2015.

[42] J. Xiong, J. He, J. Zhu et al., "Lactylation-driven METTL3-mediated RNA m^{6}A modification promotes immunosuppression of tumor-infiltrating myeloid cells," *Molecular Cell*, vol. 82, no. 9, pp. 1660–1677.e10, 2022.

[43] T. Zhang, C. Ding, H. Chen et al., "m6A mRNA modification maintains colonic epithelial cell homeostasis via NF-κB-mediated antiapoptotic pathway," *Science Advances*, vol. 8, no. 12, p. eabl5723, 2022.

[44] A. Wang, W. Tao, J. Tong et al., "m6A modifications regulate intestinal immunity and rotavirus infection," *Elife*, vol. 11, article e73628, 2022.

[45] X. Zong, X. Xiao, B. Shen et al., "TheN6-methyladenosine RNA-binding protein YTHDF1 modulates the translation ofTRAF6to mediate the intestinal immune response," *Nucleic Acids Research*, vol. 49, no. 10, pp. 5537–5552, 2021.

[46] S. Bork, S. Pfister, H. Witt et al., "DNA methylation pattern changes upon long-term culture and aging of human mesenchymal stromal cells," *Aging Cell*, vol. 9, no. 1, pp. 54–63, 2010.

[47] T. Lence, J. Akhtar, M. Bayer et al., "m^{6}A modulates neuronal functions and sex determination in _Drosophila_," *Nature*, vol. 540, no. 7632, pp. 242–247, 2016.

[48] T. Zhang, S. W. Zhang, S. Y. Zhang, S. J. Gao, Y. Chen, and Y. Huang, "m6A-express: uncovering complex and condition-specific m6A regulation of gene expression," *Nucleic Acids Research*, vol. 49, no. 20, p. e116, 2021.

[49] C. Liu, Z. Yang, R. Li et al., "potential roles of N6-methyladenosine (m6A) in immune cells," *Journal of Translational Medicine*, vol. 19, no. 1, p. 251, 2021.

[50] K. J. Yoon, F. R. Ringeling, C. Vissers et al., "Temporal control of mammalian cortical neurogenesis by m^{6}A methylation," *Cell*, vol. 171, no. 4, pp. 877–889, 2017.

[51] C. Pian, Z. Yang, Y. Yang, L. Zhang, and Y. Chen, "Identifying RNA N6-Methyladenine sites in three species based on a Markov model," *Frontiers in Genetics*, vol. 12, article 650803, 2021.

[52] Y. Yuan, G. Yan, M. He et al., "ALKBH5 suppresses tumor progression via an m^{6}A-dependent epigenetic silencing of pre-miR-181b-1/YAP signaling axis in osteosarcoma," *Cell Death & Disease*, vol. 12, no. 1, p. 60, 2021.

[53] J. Tong, R. A. Flavell, and H. B. Li, "RNA m6A modification and its function in diseases," *Frontiers in Medicine*, vol. 12, no. 4, pp. 481–489, 2018.

[54] S. Lu, Z. Yu, Z. Xiao, and Y. Zhang, "Gene signatures and prognostic values of m(6) a genes in nasopharyngeal carcinoma," *Frontiers in Oncology*, vol. 10, p. 875, 2020.

[55] T. Li, P. S. Hu, Z. Zuo et al., "METTL3 facilitates tumor progression via an m6A-IGF2BP2-dependent mechanism in colorectal carcinoma," *Molecular Cancer*, vol. 18, no. 1, p. 112, 2019.

[56] G. Bao, J. Huang, W. Pan, X. Li, and T. Zhou, "Long noncoding RNA CERS6-AS1 functions AS a malignancy promoter in breast cancer by binding to IGF2BP3 to enhance the stability of CERS6 mRNA," *Cancer Medicine*, vol. 9, no. 1, pp. 278–289, 2020.